PCCP

ROYAL SOCIETY OF CHEMISTRY

PAPER

View Article Online
View Journal | View Issue

Cite this: *Phys. Chem. Chem. Phys.*, 2023, **25**, 29993

Excess and excited-state dipole moments of real-life dyes: a comparison between wave-function, BSE/*GW*, and TD-DFT values†

Iryna Knysh, [a] Jose D. J. Villalobos-Castro, [b] Ivan Duchemin, [c] Xavier Blase *[b] and Denis Jacquemin *[ad]

In this work, we assess the accuracy of the Bethe–Salpeter equation (BSE) many-body Green's function formalism, adopting the eigenvalue-self-consistent ev*GW* exchange–correlation kernel, for the calculation of the excited-state (μ^{ES}) and excess dipole moments ($\Delta\mu$), the latter ones being the changes of dipole amplitude between the ground and excited states (ES), in organic dyes. We compare the results obtained with wave-function methods [ADC(2), CC2, and CCSD], time-dependent density functional theory (TD-DFT), and BSE/ev*GW* levels of theory. First, we compute the evolution of the dipole moments of the two lowest singlet excited states of 4-(dimethylamino)benzonitrile (DMABN) upon twisting of the amino group. Next, we use a set of 25 dyes having ES characters ranging from locally excited to charge transfer to determine both μ^{ES} and $\Delta\mu$. For DMABN our results show that BSE/ev*GW* provides $\Delta\mu$ values closer to the CCSD reference and more consistent trends than TD-DFT. Moreover, a statistical analysis of both $\Delta\mu$ and μ^{ES} for the set of 25 dyes shows that the BSE/ev*GW* accuracy is comparable or sometimes slightly better than that of TD-M06-2X and TD-CAM-B3LYP, BSE/ev*GW* outperforming TD-DFT in challenging cases (zwitterionic and cyanine transitions). Finally, the starting point dependency of BSE/ev*GW* seems to be larger for $\Delta\mu$, ES dipoles, and oscillator strengths than for transition energies.

Received 14th September 2023,
Accepted 18th October 2023

DOI: 10.1039/d3cp04467j

rsc.li/pccp

1 Introduction

The excited-state (ES) dipole moment (μ^{ES}) is an important molecular property that characterizes the electronic nature of the ES. For instance, μ^{ES} can be used to explain the differences in molecular absorption and emission spectra, including the shifts and broadening induced by the polarity of the solvent, an effect known as solvatochromism.[1] Additionally, the dipole moment can be viewed as a tool to quantify intermolecular interactions,[2] *e.g.*, it was recently shown that studying the dipole–dipole interactions in the ES and ways to suppress them can lead to more efficient thermally activated delayed fluorescence (TADF) diodes.[3] The dipole moments also play an important role in the investigation of the mechanism of dual fluorescence of 4-(dimethylamino)benzonitrile (DMABN, see Fig. 1).[4] This molecule is characterized by an emission from a local excited (LE, ^1L_b-type) state in non-polar solvents. However, in polar environments, an additional redshifted fluorescence band appears and is assigned to the emission from a state possessing a strong intramolecular charge transfer (CT) character (^1L_a-type). According to the twisted intramolecular charge transfer (TICT) model,[5–7] the CT state is formed by twisting the amino group perpendicularly to the benzene ring in the ES. The theoretical study of the TICT mechanism by Georgieva *et al.*[8] reported a large dipole moment for the CT state as compared to

[a] *Nantes Université, CNRS, CEISAM UMR 6230, F-44000 Nantes, France. E-mail: Denis.Jacquemin@univ-nantes.fr*
[b] *Université Grenoble Alpes, CNRS, Institut Néel, F-38042 Grenoble, France. E-mail: xavier.blase@neel.cnrs.fr*
[c] *Université Grenoble Alpes, CEA, IRIG-MEM-L_Sim, 38054 Grenoble, France*
[d] *Institut Universitaire de France, F-75005 Paris, France*

† Electronic supplementary information (ESI) available: (i) Additional computational details for the BSE/ev*GW* finite-field calculations; (ii) MOs participating in the transitions for the three lowest ES of DMABN for CC2, ADC(2), TD-DFT, and BSE/ev*GW* methods; (iii) μ^{GS}, ΔE, f, and μ^{ES} data for all compounds; (iv) Cartesian coordinates. See DOI: https://doi.org/10.1039/d3cp04467j

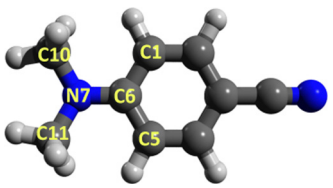

Fig. 1 Structure of DMABN molecule with numbering of the atoms defining the key dihedral angles (C1–C6–N7–C10 and C5–C6–N7–C11).

the ground state (GS) dipole (μ^{GS}). This leads to stronger interactions with the polar medium that allow stabilizing the CT state in the TICT conformation.

The experimental determination of μ^{ES} is complicated. In most cases, ES dipole moments are obtained using either rotationally resolved electronic Stark spectroscopy or solvatochromic shift measurements. The first method deduces permanent dipole moments from the field-induced shifts of line positions in the vibronic spectra.[9,10] This type of experiment is characterized by high resolution and conducted in the gas phase. However, this method is limited to compact systems and allows estimating the dipole moments of isolated molecules only. In contrast, in solvatochromic measurements, as seen from the name, the molecules are perturbed by the field of the solvent. This method is based on measures of the absorption and fluorescence maxima in different solvents, which are next analyzed using the so-called Lippert–Mataga equation.[11,12] This equation is based on Onsager's reaction field theory, where the dye is modeled as a point dipole at the center of the spherical cavity.[10] Obviously, this is far from reality for most real-life molecules. This has stimulated the implementation of other equations aiming to correct the problems arising in Lippert–Mataga's theory, for example, by accounting for the solvent–solute interactions through empirical coefficients.[10,13–15] In any case, the approximations used in solvatochromic models typically result in significantly overestimated ES dipole moments.[9,10,16]

Another way to determine the ES dipole moments is by using theoretical methods. Either one has to use a level of theory providing the ES density or rely on the finite-field (FF) approach (applying an electric field and performing numerical derivation of the energies). Obviously, the calculation of the ES dipole moments always adds an additional cost compared to the energy calculations and this is the bottleneck for the theoretical methods. For small molecules (up to 20–25 atoms), the highest level of theory that can be applied in practice is coupled-cluster singles and doubles (CCSD).[17,18] For larger dyes (up to 70–80 atoms) the best references are usually determined with second-order CC (CC2)[19] or algebraic diagrammatic construction [ADC(2)][20,21] methods. Additionally, for ES calculation, one can choose between the linear-response (LR) formalism that can be applied to all above-mentioned theories,[22–24] the equation-of-motion (EOM) method for CC2 and CCSD levels,[25,26] and the intermediate state representation (ISR) for ADC theories.[27,28] Moreover, the wave-function calculation of the μ^{ES} can be achieved using the orbital-relaxed (OR) and orbital-unrelaxed (UR) approaches.[29,30] More detailed discussions of both the nature and impact of these formalisms can be found elsewhere.[31,32]

In light of the computational cost of wave-function methods, time-dependent density functional theory (TD-DFT) remains a widely used method for determining ES energies and properties, including μ^{ES}.[33–35] In practice, the main drawback of TD-DFT is its dependence on the chosen exchange–correlation functional (XCF) that can result in inaccurate μ^{ES}, especially for the ES states having a CT character.[32,36–40] The Bethe–Salpeter equation (BSE) formalism,[41–48] that provides an accurate description of screened non-local electron–hole interactions, can be viewed as an alternative to TD-DFT. BSE, in connection with many-body *GW* theory,[49–52] was shown to correctly predict the energies of CT states as well as the transition energies of cyanine derivatives,[53–60] two types of states challenging for TD-DFT. Moreover, the (starting) XCF dependency can be significantly reduced when using the so-called eigenvalue-self-consistent *GW* scheme (ev*GW*)[61,62] that implies a self-consistent update of the eigenvalues while keeping the molecular orbital coefficients (eigenvectors) frozen. Over the last few years, BSE has been applied beyond transition energies and its accuracy has been evaluated for a few ES properties including oscillator strengths and ES geometries (using numerical forces, approximated gradients, and potential energy surface with reduced dimensionality).[63–69] In our recent work we showed using a FF approach that BSE/ev*GW* provides accurate trends for the evolution of the excess dipole moments ($\Delta\mu$, the difference between ES and GS dipoles) of increasingly long push–pull chains.[70] Additionally, an approximation to BSE analytical gradients within an adapted Lagrangian *Z*-vector approach[71,72] for calculating dipole moments was proposed by us very recently.[73] Such a formalism allows evaluating all gradients at the cost of a single ES calculation, a much cheaper approach as compared to finite-field schemes. A benchmark on a set of tiny molecules and the above-mentioned push–pull chains has shown that this approximated analytical (AA) scheme performs as well as the "best" XCF in TD-DFT for complicated cases such as Rydberg and CT transitions. To the very best of our knowledge, these two previous works[70,73] are the only ones to treat ES dipole moments at the BSE/*GW* level.

In the present work, we use both the FF approach and the AA scheme in order to explore the performance of the BSE/ev*GW* formalism for ES dipoles of realistic molecules. We compare our results to both TD-DFT and wave-function data. We divide the discussion of the results into two parts: (i) first we study the evolution of the excess dipoles upon the twist for the lowest singlet ES of DMABN; (ii) next, we compare the excess dipole moments for a set of 25 conjugated molecules having an ES character ranging from strongly localized to strongly charge-transfer (Fig. 2), and also containing cyanine and zwitterionic examples.

2 Computational details

The total GS and ES dipole moments as well as excess dipoles that we list below have been determined using the following formulas:

$$\mu^{GS} = \sqrt{\left(\mu_x^{GS}\right)^2 + \left(\mu_y^{GS}\right)^2 + \left(\mu_z^{GS}\right)^2}, \quad (1)$$

$$\mu^{ES} = \sqrt{\left(\mu_x^{ES}\right)^2 + \left(\mu_y^{ES}\right)^2 + \left(\mu_z^{ES}\right)^2}, \quad (2)$$

$$\Delta\mu = \sqrt{\left(\mu_x^{ES} - \mu_x^{GS}\right)^2 + \left(\mu_y^{ES} - \mu_y^{GS}\right)^2 + \left(\mu_z^{ES} - \mu_z^{GS}\right)^2}. \quad (3)$$

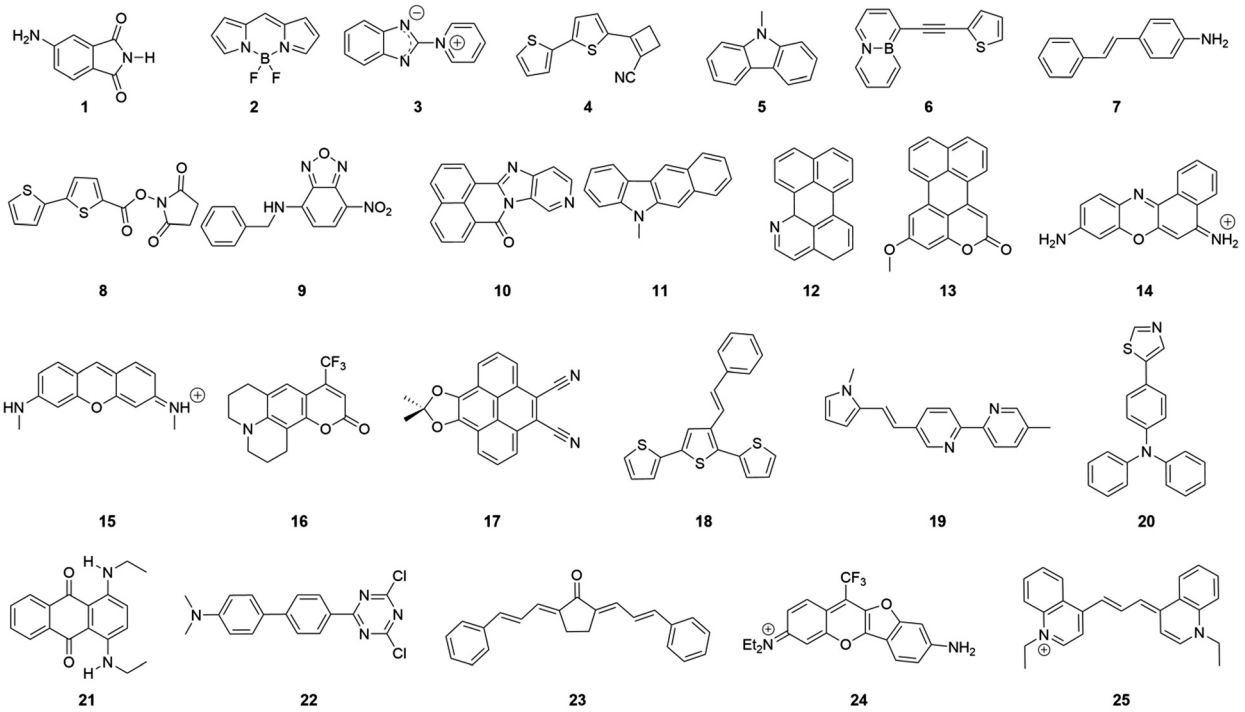

Fig. 2 Structural representation of the molecules considered in the dye set.

Since the $\Delta\mu$ values do not account for the sign of the dipole moments, we highlight below in italics the cases where the difference between μ^{ES} and μ^{GS} are negative.

2.1 DMABN twist

The set of interpolated geometries showing a twist angle going from 0° to 90° by 10° steps was taken from a previous work[68] and are reproduced in the ESI.† The calculation of the GS and ES dipole moments have been done using the cc-pVTZ atomic basis set. The resolution of identity (RI)[74] approach has been employed to determine orbital-relaxed EOM-CCSD dipoles using the Q-Chem 6.0.1 code.[75] In these calculations the following parameters were improved from default ones: (i) self-consistent field convergence was changed to 10^{-11}; (ii) the integral threshold was changed to 10^{-14}; (iii) the CC GS convergence was set to 10^{-9} and the EOM-CCSD convergence to 10^{-7}; and (iv) the Davidson diagonalization threshold was set to 10^{-5}. RI-LR-CC2 and RI-LR-ADC(2) calculations have been done accounting or not for the orbital relaxation using the Turbomole 7.5 code.[76,77] The default convergence criteria were used in these calculations. TD-DFT calculations have been performed with the Gaussian16 program[78] and its default options using four XCF including a semilocal GGA (PBE),[79] a popular global hybrid (PBE0),[79,80] a tuned PBE0 with 54% of exact exchange (referred to as PBEh), and a range-separated hybrid (CAM-B3LYP).[81] We chose the PBEh functional with constant percentage of exact exchange in this case as tuning the PBE0 functional on each geometry (each dihedral) might lead to non-smooth evolutions.

BSE/ev*GW* calculations of dipole moments have been done applying both the FF approach and the recently developed AA method using the beDeft (beyondDFT) package,[82,83] starting with Kohn–Sham PBE0 eigenstates. Even though significantly more tedious and expensive, the FF values provide the BSE/ev*GW* reference. The Lagrangian *Z*-vector AA approach introduces the numerically efficient simplification that the quasiparticle ev*GW* energy level gradients are replaced by their Kohn–Sham analogs in the *Z*-vector eigensystem to be solved.[63,73] Such an approximation introduces a larger dependence on the starting point functional as compared to the FF approach. As shown in ref. 73, the impact of this approximation can be significantly reduced by adopting an optimally tuned functional equating the ev*GW* and Kohn–Sham highest-occupied-molecular-orbital (HOMO) energies. In the case of DMABN, we used the PBEh global hybrid that showed better performance than PBE0 in the case of extended push–pull oligomers.[70] Analytic BSE/ev*GW*/PBEh gradients are thus provided together with their BSE/ev*GW*/PBE0 analogs for the sake of comparison. The Coulomb-fitting RI[84] is implemented in the beDeft package and was used, adopting the cc-pVTZ-RIFIT auxiliary basis set.[85] For the FF calculations, electric fields of $\pm$0.00025 and $\pm$0.0005 a.u. were applied along the three Cartesian axes during the DFT calculations (using PBE0 and PBEh XCF) in the ORCA 5.1 program.[86] The obtained electric-field-dependent Kohn–Sham (KS) eigenstates served as starting points for BSE/ev*GW* calculations. We explicitly corrected the 3 highest occupied and 5 (3) lowest virtual eigenvalues at the ev*GW*/PBE0 (ev*GW*/PBEh) level, while lower occupied/higher virtual levels were rigidly shifted following the explicitly

corrected lowest/highest level, respectively. These choices are adequate since the considered ES involve only the orbitals around the gap. The FF μ^{ES} were estimated as described in the ESI.† During the much more efficient AA calculations, all the occupied and virtual states within 10 eV gap were explicitly corrected at the ev*GW* level, yielding results in close agreement with values obtained correcting explicitly 3 highest occupied and 5 (3) lowest virtual eigenvalues.

In order to quantify the LE and CT characters of the ES we calculated Bahers' CT distance (D_{CT})[87,88] at the TD-CAM-B3LYP/cc-pVTZ level of theory using Gaussian 16.

2.2 Set of dyes

The GS geometries of the 25 dye molecules (see Fig. 2) optimized at the M06-2X/6-31+G(d) level of theory have been taken from a previous work,[89] and the Cartesian coordinates can be found in the ESI.† Most of the molecules in the set have been used in the previous benchmark of dipole moments with various TD-DFT approximations.[40] As stated in the Introduction, this set offers a large panel of different ES characters. All dipole moment calculations have been carried out using the cc-pVTZ atomic basis set. This basis set was chosen considering the size of the studied systems and applied levels of theory. Additionally, we did a small benchmark for three medium-sized molecules from our set (**8**, **9**, and **10**), which shows that cc-pVTZ is an adequate choice for these systems (see Table S22 in the ESI†). Except when specified, we focus on the response of the first singlet ES. The RI-EOM-CCSD/cc-pVTZ calculations were possible for the smallest molecules only, which is why we did the CCSD calculation for bigger molecules using the smaller cc-pVDZ atomic basis set, adding the basis set correction obtained at the CC2 level ($\mu_{CC2}^{cc\text{-}pVTZ} - \mu_{CC2}^{cc\text{-}pVDZ}$) to estimate the cc-pVTZ EOM-CCSD results. CCSD calculations have been done using the Q-Chem 6.0.1 program with the same options as mentioned above. RI-LR-CC2 and RI-LR-ADC(2) calculations have been performed using both OR and UR approaches with the aid of the Turbomole 7.5 package. TD-DFT dipole moments were determined with Gaussian16 using six XCF: PBE,[79] PBE0,[79,80] PBEh (PBE0 with 54% exact exchange), M06-2X,[90] CAM-B3LYP,[81] and ωB97X-D.[91] BSE/ev*GW* dipole moments have been obtained with the FF approach as well as with the AA scheme using the beDeft code. In the finite difference approach, we used PBE0 as a starting point. Consistent with the above discussion of the DMABN case, for the approximate analytic AA scheme, we additionally used KS eigenstates obtained with PBEh and an optimally tuned PBEα global hybrid functional (α% of exact exchange determined for each compound are given in the ESI†). At the FF ev*GW*/PBE0 level, we explicitly corrected 5 highest occupied and 5 lowest virtual eigenvalues, except for a few cases (see the ESI†). For the AA calculations, we explicitly corrected at the ev*GW* level all the occupied and virtual states within 10 eV gap, showing good agreement with calculations performed correcting explicitly 5 occupied/virtual levels.

In this work, we used statistical analysis to evaluate the accuracy of the $\Delta\mu$ calculated at different levels of theory. In more detail, we determined the mean absolute error (MAE), mean signed error (MSE), standard deviation of the errors (σ), maximal positive [Max(+)] and negative [Max(−)] deviations, Pearson correlation coefficient (R), Spearman rank-order correlation coefficient (ρ), and linear determination coefficient (R^2).

3 Results and discussion

3.1 Dipole moments upon the DMABN twist

In previous studies, it was shown that some DFT approximations are badly failing to reproduce the correct topology of the ES potential energy surfaces (PES) along the twist coordinate of the amino group of DMABN, whereas BSE provides accurate PES.[68,92] Here we compare the evolution of the dipole moments for the two lowest singlet ES of this compound during the twist using various levels of theory. Before going into the discussion of the dipole moments let us first take a look at Fig. 3, which presents the Hartree–Fock molecular orbitals (MOs) participating in the transitions to the **1B**, **2A**, and **2B** ES as given by the CCSD/cc-pVTZ level of theory. The MOs for CC2, ADC(2), TD-DFT (PBE, PBE0, PBEh, and CAM-B3LYP), and BSE/ev*GW* (starting with PBE0 and PBEh) methods can be found in the ESI.† Additionally, in Fig. S5 (ESI†) we list the D_{CT} values calculated at the TD-CAM-B3LYP level of theory. From the MOs in Fig. 3 one notices that the first ES (**1B**) at the untwisted geometry corresponds to a π–π* transition from the delocalized HOMO orbital to the phenyl-localized LUMO+1, indicating a LE nature. The second ES (**2A**) at this geometry is a HOMO–LUMO π–π* transition with both orbitals being delocalized over the whole molecule. This state has a slight CT character and its D_{CT} amplitude is twice larger than for **1B** (see also Fig. S5, ESI†). During the twist, the orbitals evolve which results in a clear CT character for both **2A** and **1B** states at the twisted geometry. Additionally, in Fig. 3 we also present the MOs for the third ES (**2B**); this state is a Rydberg ES at the untwisted geometry, but upon rotation of the NME_2 group, it transforms into a localized

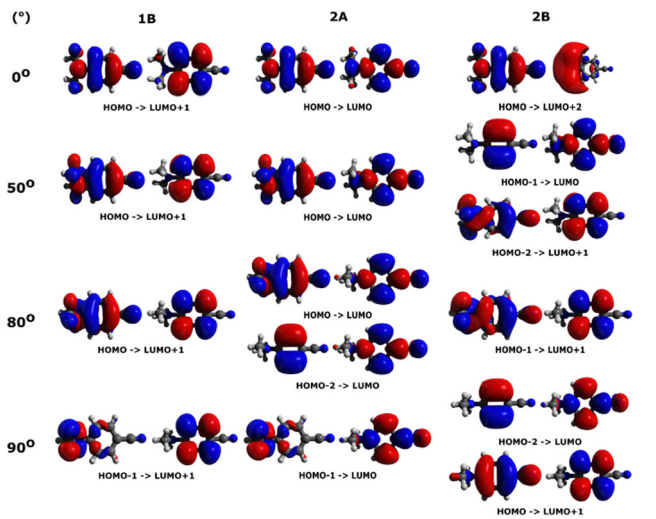

Fig. 3 Hartree–Fock MOs participating in the transitions of the **1B**, **2A**, and **2B** ES (S_1, S_2, and S_3 respectively at the untwisted geometry) determined at the CCSD/cc-pVTZ level of theory.

π–π* transition. Below, we mainly discuss $\Delta\mu$ and μ^{ES} of DMABN, although the data for the μ^{GS}, transition energies (ΔE), and oscillator strength (f) can be found in the ESI.†

Let us start our analysis by a comparison of the $\Delta\mu$ obtained using wave-function, TD-DFT, and BSE/ev*GW* methods for the **1B** state (see Fig. 4), which is a LE state at the planar geometry but gains a significant CT character at large dihedral angles. The UR approach tends to overestimate the dipole moments, and thus we do not discuss UR results in this manuscript, but the corresponding data is available in the ESI.† In the case of wave-function methods, significant differences can be seen between the relaxed approaches when comparing CC2 [or ADC(2)] and CCSD results. Moreover, these differences increase with the twist angle, the latter method always giving significantly smaller $\Delta\mu$ but at 90°. Indeed starting at a 60° twist, CCSD provides a completely different behavior with an unexpected kink at 80°. In order to explain this unusual behavior let us go back to the discussion of the MOs participating in the ES transitions. In Fig. 3 one can notice the high similarity between the topologies of the MOs contributing to both **1B** and **2B** states at 80° twist. However, it is not the case for CC2 nor ADC(2), which predict different sets of localized MOs for the **1B** and **2B** transitions (see Fig. S1 in the ESI†). This is because, at the CCSD level the **1B** and **2B** states are nearly degenerated whereas they are not with second-order methods. In Table 1 (see more methods in the ESI†) we present the energy differences between **1B** and **2B** states. During the twist, the energetic gap between the two lowest B states is reduced with all methods reported here. In the case of CCSD at 90° structure, these two states are even switched and the ΔE_{diff} become negative. In contrast, CC2 and ADC(2) predict the two B states to be more than 0.5 eV apart even at highly twisted geometries. In a previous study of the six lowest singlet ES of *N*-phenylpyrrole (N-PP),[69] we observed a similar behavior: the PES of the 5th and 6th ES of N-PP are extremely close one from another with both CCSD and CCSD(T)(a)* (with perturbative triples),[93] whereas a large gap between them is found with CC2. That is the reason behind the smooth $\Delta\mu$ CC2 trends for the **1B** state and the kinked one with CCSD.

Table 1 Energy difference between **2B** and **1B** states (ΔE_{diff})[a] obtained at CCSD, CC2, TD-DFT (PBE and PBEh), and BSE/ev*GW*/PBE0 levels of theory using the cc-pVTZ atomic basis set. See the ESI for other methods

	ΔE_{diff}^{CCSD}	ΔE_{diff}^{CC2}	ΔE_{diff}^{PBE0}	ΔE_{diff}^{PBEh}	$\Delta E_{diff}^{BSE/evGW/PBE0\ b}$
0°	1.55	1.49	1.27	1.56	1.64
10°	1.56	1.50	1.29	1.57	1.62
20°	1.57	1.51	1.33	1.58	1.56
30°	1.56	1.50	1.38	1.50	1.46
40°	1.50	1.47	1.40	1.37	1.31
50°	1.30	1.30	1.31	1.19	1.11
60°	1.03	1.09	1.22	0.95	0.85
70°	0.72	0.86	1.14	0.67	0.55
80°	0.39	0.65	1.10	0.35	0.26
90°	−0.14	0.57	1.10	−0.03	0.06

[a] $\Delta E_{diff} = E_{2B}^{tot} - E_{1B}^{tot}$. [b] The results obtained with the 3&5 correction scheme at ev*GW* level. See more details in the ESI.

In order to show how state mixing can affect the dipole moments let us briefly discuss the third ES (**2B**). As seen from Fig. 3, at small twist angles, a Rydberg character is clear, whereas, at larger angles, the MOs indicate a LE character when relying on CCSD. However, as can be seen from the MOs contributions obtained with other levels of theory some of them result in pure Rydberg (TD-PBE) or almost pure LE (BSE/ev*GW*, except for the untwisted structure) transitions for **2B** state (see Fig. S1–S7, ESI†). This results in significant differences between the different methods for the energies (see Fig. S11, ESI†), but more importantly the evolution of the dipole moments is getting impossible to track for **2B** as can be seen in Fig. S17 and S20 (ESI†).

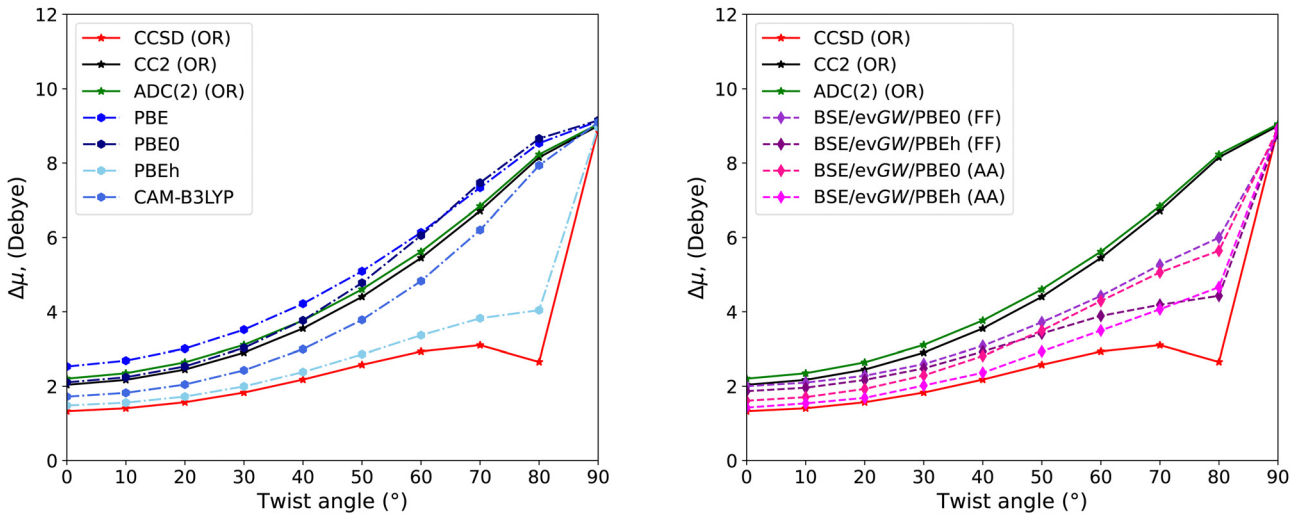

(a) TD-DFT **(b)** BSE/evGW

Fig. 4 Evolution upon twisting of the $\Delta\mu$ of the **1B** ES of DMABN using (a) TD-DFT with PBE, PBE0, PBEh, and CAM-B3LYP functionals and (b) BSE/ev*GW* using PBE0 and PBEh as starting points compared to the wave-function methods including CCSD, CC2, and ADC(2). OR stands for the orbital-relaxed approach. FF (AA) indicates that the dipole moments were computed with the finite-field (approximated analytical gradients) approach.

Let us now come back to the discussion of the $\Delta\mu$ of the **1B** state with TD-DFT and BSE/ev*GW* methods. In Fig. 3 we can notice different behaviors among the XCF used in this work (PBE, PBE0, PBEh, and CAM-B3LYP). However, these differences are not as dramatic as for the PES.[68,92] TD-PBE and TD-PBE0 show a slight overestimation of the excess dipoles compared to the CC theories, while TD-CAM-B3LYP and TD-PBEh are between CC2 and CCSD. Interestingly, only PBEh with 54% of exact exchange is reproducing the specific behavior of CCSD $\Delta\mu$ due to the energetically close B states at the twisted geometry (see Table 1). In contrast, the $\Delta\mu$ obtained with the various BSE/*GW* formalisms (Fig. 3) show evolutions of the excess dipoles always rather similar to that of CCSD. This can be also explained by a small gap between the two B states with the BSE/ev*GW* formalism (see Table 1 and Table S2 in the ESI†). Additionally, we can notice a rather significant impact of the KS starting point (PBE0 *versus* PBEh), especially in the large twist region. The closest agreement with the CCSD reference is obtained using the PBEh MOs in the BSE/ev*GW* procedure. Finally, BSE/ev*GW* dipoles determined using approximated analytical gradients tend to be slightly smaller than the ones obtained with the FF approach, but the key trends remain independent of the approach used to compute the BSE/ev*GW* $\Delta\mu$ (FF or AA). Generally, one observes similar trends for μ^{ES} (Fig. S15, ESI†) as for the excess dipoles in Fig. 4, except for the more noticeable overestimation of CC2 μ^{ES} values by TD-PBE and TD-PBE0 functionals.

Let us now turn to the evolution of the dipole moments upon twisting for the **2A** state, the CT ES. The $\Delta\mu$ graphs for this state obtained with wave-function methods, TD-DFT, and BSE/ev*GW* are presented in Fig. 5. In contrast with **1B** state, all the wave-function methods with the OR approach provide $\Delta\mu$ that are quite close to each other for this ES. Nevertheless, CCSD is giving smaller excess dipoles than CC2, while ADC(2) yields slightly larger values. Similar trends for these two levels of theory were found for the dipole moments of long push–pull chains.[70] As for the **1B** ES the $\Delta\mu$ are not showing the dramatically different behavior found for the PES when using different XCF. Both TD-DFT and BSE/ev*GW* results show an underestimation of the $\Delta\mu$ at small twist angles compared to CCSD, while at larger twists, the trend is reversed. In the BSE case, one sees smaller differences between the PBE0 and PBEh results than with the TD-DFT approach. Finally, we can compare the BSE/ev*GW* dipole moments computed with the FF and AA approaches. As can be seen from Fig. 4 the latter scheme tends to underestimate the dipoles as compared to the (non-approximated) FF method, except at large twist angles where the FF and AA results cross. However, this underestimation is rather systematic, meaning that the difference between the analytic and numerical dipole moments is rather independent from both the starting functional and twisting angle. On the other hand, no major difference can be pinpointed between the evolution of $\Delta\mu$ (Fig. 5) and μ^{ES} (Fig. S16, ESI†) values: the key trends are similar. Nevertheless, we note that the difference between CCSD and CC2 values is slightly larger in the case of μ^{ES} than $\Delta\mu$.

In the discussions above we compared the performance of the different methods for predicting the $\Delta\mu$ of the two lowest ES of DMABN during the twist, but it is also interesting to check how these methods reproduce the difference between the $\Delta\mu$ values of the **1B** and **2A** ES ($\Delta\mu^{diff}$). The results obtained with TD-DFT and BSE/ev*GW* approaches are compared to CC2 and CCSD values in Fig. S21 (ESI†). Globally, it is seen that both TD-DFT and BSE/ev*GW* provide smaller $\Delta\mu^{diff}$ than CC theories. Moreover, we can clearly see that the evolution of the $\Delta\mu^{diff}$ given by TD-PBE and TD-PBE0 resembles neither their CC2 nor CCSD counterparts. In contrast, TD-CAM-B3LYP is following the CCSD evolution of $\Delta\mu^{diff}$ at small twists, but becomes very close to CC2 at larger twists. Only TD-PBEh is always showing a

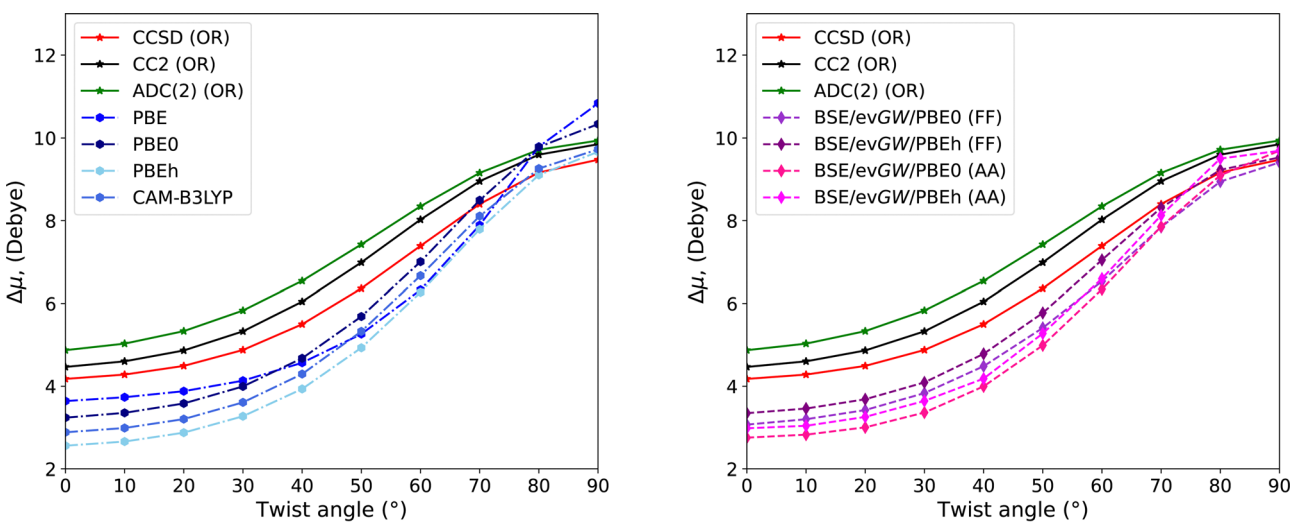

(a) TD-DFT **(b)** BSE/evGW

Fig. 5 Evolution of the $\Delta\mu$ of the **2A** ES using (a) TD-DFT and (b) BSE/ev*GW* formalisms compared to the wave-function methods. See the caption of Fig. 4 for more details.

consistent trend with CCSD results. In contrast, all the BSE/ev*GW* $\Delta\mu^{diff}$ curves are rather parallel to their CCSD counterparts, regardless of the approach used to compute the dipole moments. Furthermore, there is almost no difference between AA and FF $\Delta\mu^{diff}$ when PBEh is used as a starting point.

In short, we have seen a clear trend of significant increase of $\Delta\mu$ upon twisting for the CT **2A** ES, all methods providing quite similar values with the BSE/ev*GW* curves parallel to the CC2 and CCSD ones albeit with a slight underestimation tendency. For the **1B** ES, the presence or absence of state-mixing makes the comparison more difficult, though we noticed that BSE/ev*GW* and EOM-CCSD evolutions are highly similar.

3.2 Dipole moments of the dyes

The excess dipole moments of the 25 dyes shown in Fig. 2 calculated using wave-function [CCSD, CC2, and ADC2(2)], TD-DFT (PBE, PBE0, PBEh, M06-2X, ωB97X-D, and CAM-B3LYP), and BSE/ev*GW* (starting with PBE0, PBEh, and PBEα) levels of theory are listed in Table 2. The μ^{GS}, ΔE, f, and μ^{ES} values can be found in the ESI,† together with results obtained applying the UR approach for CC2 and ADC(2) methods. In Table 2 we also present the charge transfer distance (D_{CT}) for each of the transitions considered. Most of the ES transitions can be characterized as $\pi \rightarrow \pi^*$ excitations varying between strong LE (**12** and **25**) to strong CT character (**3** and **22**). Nevertheless, we also consider four cyanine-like molecules (**14**, **15**, **24**, and **25**). As found for DMABN, CC2 (OR) and ADC(2) (OR) provide $\Delta\mu$ that are quite close to each other, and the discrepancies increase with the UR scheme (see Table S13, ESI†). On the other hand, larger differences are seen between CCSD and CC2 dipoles, the former usually delivering smaller dipole moments than the latter. Additionally, an underestimation of the $\Delta\mu$ compared to CC theories can be seen with the RSH functionals in TD-DFT as well as with BSE/*GW*. Again we notice that TD-DFT (ωB97X-D and CAM-B3LYP) and BSE/ev*GW* results are closer from the CCSD values than from the CC2 ones. Similar trends were previously observed for the $\Delta\mu$ evolution of long push–pull oligomers.[70] Moreover, we can observe a correlation between the increase of the D_{CT} parameter and the increase of $\Delta\mu$ differences between various levels of theories: CT transitions are indeed more challenging to model than local excitations.

Let us first discuss a few interesting examples from Table 2 (highlighted in bold) for which quite significant discrepancies are seen between various methods. The first is molecule **3** that presents a zwitterionic character and has also two low-lying ES with quite significant CT characters (large D_{CT}) and large $\Delta\mu$ values. CCSD provides excess dipoles for those states *ca.* 1 D smaller than CC2, while ADC(2) overshoots the CC2 values. Moreover, a more significant difference is seen between these methods for the μ^{ES} (>2 Debye) in Table S10 (ESI†). Additionally, extremely low $\Delta\mu$ values compared to CC values are obtained with both TD-PBE and TD-PBE0 functionals for the A_1 ES, whereas for the B_1 state the errors become smaller, especially with TD-PBE0. Interestingly, increasing the amount of exact exchange in PBE0 functional (TD-PBEh) provides a $\Delta\mu$ (9.10 D) close to the CC references. The Minnesota (TD-M06-2X) and RSH (TD-CAM-B3LYP and TD-ωB97X-D) XCF also underestimate the excess dipoles of both states compared to the CC values, with especially large differences for the A_1 ES. Comparing μ^{ES} values for TD-DFT methods (Table S11, ESI†), one can notice that for A_1 ES, GGA and global hybrids functionals tend to overestimate CCSD dipoles, while other functionals provide more than 1 Debye lower values. On the other hand more accurate μ^{ES} values are obtained with TD-PBEh, TD-M06-2X, and RSH functionals for the B_1 state. In contrast, BSE/ev*GW*/PBE0 (FF) and BSE/ev*GW*/PBEα (AA) $\Delta\mu$ values are in good agreement with both CCSD and CC2 references, outperforming TD-DFT irrespective of the selected XCF. Nevertheless, from molecule **3**, the approximated BSE/ev*GW* analytical gradient scheme relying on PBE0 (PBEh) MOs leads to results similar to the TD-PBE0 (TD-PBEh) ones for both $\Delta\mu$ and μ^{ES} (see Table 2 and Tables S10–S12, ESI†). This is the signature of approximating the ev*GW* quasiparticle energy gradients by their Kohn–Sham analogs, leading to an intermediate scheme that properly relies on the BSE electron–hole interaction gradients but adopts the Kohn–Sham hole and electron energy evolution under the external electric field.

Another interesting case is dye **14** that is also non-centrosymmetric and has a quite low D_{CT} value consistent with a cyanine excitation. Significant differences can be seen when comparing CC2 with CCSD or ADC(2) $\Delta\mu$ excess dipoles, with deviations of the order of 0.77 D and 0.70 D, respectively. As for the previous molecule, TD-DFT tends to underestimate the excess dipole, and significantly too low values are obtained with both TD-PBE and TD-PBE0. In contrast, BSE/ev*GW*/PBE0 (FF) perfectly matches the CC2 result, while underestimating by 0.79 D the CCSD value. It is also worth mentioning that among all the methods, BSE/ev*GW*/PBE0 (FF) provides the closest μ^{ES} from the CCSD reference (see Tables S10–S12 in the ESI†). For the BSE/ev*GW* analytical dipoles, it is seen that using PBEα as a starting point allows improving the results as compared to a PBE0 starting point.

A third case is molecule **22** that has the strong CT transition (D_{CT} = 4.13 Å) and consistently a large $\Delta\mu$. A large overestimation (4.49 D) of the $\Delta\mu$ is given by the CC2 when considering CCSD as a benchmark. Additionally, all the other methods presented in Table 2 with the exception of ADC(2) also give $\Delta\mu$ smaller than CC2. Among the TD-DFT results, we can notice that the TD-PBE0 excess dipole is the closest to the CC2 one, whereas TD-PBE and TD-M06-2X provide $\Delta\mu$ values closer to CCSD; RSH XCF showing slightly lower $\Delta\mu$. The BSE/ev*GW*/PBE0 (FF) excess dipole for molecule **22** is close to the CCSD reference and is bracketed by the TD-M06-2X and TD-CAM-B3LYP values, while BSE/ev*GW* analytical dipoles are closer to the TD-PBEh and TD-ωB97X-D results. One can see similar trends for the μ^{ES} values in Tables S10–S12 (ESI†). In our previous work,[70] we also observed a significant underestimation of the excess dipole moments by both TD-DFT (RSH functionals) and BSE/ev*GW* methods compared to CC2 data for strong CT cases. However, we also reported a large decrease of $\Delta\mu$ between CC2 and CCSD. In short, in these three complicated cases of zwitterionic, cyanine, and strong CT transitions,

Table 2 Excess dipole moments (in Debye) for the dye set obtained with wave-function [CCSD, CC2, and ADC(2)], TD-DFT (PBE, PBE0, PBEh M06-2X, CAM-B3LYP, and ωB97X-D), and BSE/ev*GW* (PBE0, PBEh and PBEα) approaches using the cc-pVTZ atomic basis set. The D_{CT} values have been calculated using CAM-B3LYP/cc-pVTZ level of theory. FF (AA) indicates that the dipole moments were obtained using a finite-field (approximated analytical gradients) approach. OR stands for the relaxed approach used to calculate dipoles. See the ESI for UR values. The data highlighted in bold are discussed in the text. The values in italic highlight that the difference between the total μ^{ES} and μ^{GS} is negative

			Δμ, [D]												
	State	D_{CT} [Å]	CCSD (OR)	CC2 (OR)	ADC(2) (OR)	PBE	PBE0	PBEh	M06-2X	CAM-B3LYP	ωB97X-D	BSE/*GW*/PBE0[d]	BSE/*GW*/PBE0[e]	BSE/*GW*/PBEh[f]	BSE/*GW*/PBEα[g]
1	A (π → π*)	1.53	2.75	3.88	3.78	4.67	4.58	3.79	3.01	3.98	3.90	3.79	3.72	3.73	3.68
2	B_2 (π → π*)	0.23	*0.34*	*0.18*	*0.23*	*0.21*	*0.26*	*0.44*	*0.36*	*0.38*	*0.40*	*0.34*	*0.23*	*0.52*	*0.65*
3	A_1 (π → π*)	***2.88***	***11.29***	***12.40***	***13.63***	***4.24***	***5.83***	***9.10***	***8.62***	***8.76***	***9.19***	***10.33***	***5.57***	***9.06***	***10.45***
	B_1 (π → π*)	**2.75**	***12.85***	***13.68***	***14.27***	***7.56***	***10.05***	***12.49***	***12.07***	***11.94***	***11.89***	***14.05***	***10.05***	***12.40***	***13.32***
4	A (π → π*)	1.32	3.93	5.01	5.11	5.57	3.42	2.26	2.87	2.49	2.29	2.61	2.18	2.32	2.34
5	A′ (π → π*)	0.46	0.70	0.96	1.06	1.16	1.12	0.96	0.99	1.00	1.02	0.90	0.92	0.92	0.91
6	A′ (π → π*)	0.94	*0.64*	*2.59*	*2.05*	8.90	4.04	*1.53*	*2.24*	*1.80*	*1.61*	*1.83*	*1.70*	*1.40*	*1.25*
7	A (π → π*)	1.66	1.92[c]	4.92	5.06	8.01	5.00	2.91	3.66	3.28	3.01	2.89	2.80	2.91	2.86
8	A (π → π*)	1.64	4.95[c]	5.55	5.65	4.63	4.42	3.13	3.83	3.45	3.22	2.38	3.08	3.28	3.29
9	A (π → π*)	1.15	4.39[c]	4.11	4.51	3.07	2.72	2.40	2.74	2.65	2.66	2.97	2.42	2.55	2.56
10	A′ (π → π*)	1.10	*1.21*[c]	*3.18*	*3.16*	*6.68*	*4.99*	*2.48*	*2.59*	*2.46*	*2.20*	*2.27*	*2.66*	*2.29*	*2.16*
11	A (π → π*)	0.73	1.23[c]	1.82	1.90	2.20	1.85	1.44	1.68	1.65	1.65	1.69	1.54	1.38	1.31
12	A′ (π → π*)	0.08	0.91[c]	0.75	0.82	0.14	0.07	0.11	0.17	0.13	0.17	0.26	0.07	0.10	0.17
13	A′ (π → π*)	0.65	1.85[c]	2.02	1.88	4.96	1.82	1.03	1.27	1.19	1.15	1.38	1.39	1.25	1.22
14[b]	A′ (π → π*)	**0.54**	**2.24**[c]	**1.47**	**2.17**	***0.47***	***0.53***	**0.94**	**1.05**	**0.97**	**1.03**	**1.45**	**0.70**	**1.03**	**1.14**
15[b]	B_2 (π → π*)	0.70	1.30[c]	1.33	1.52	1.28	1.33	1.34	1.33	1.32	1.35	1.21	1.12	1.47	1.55
16	A (π → π*)	1.94	6.04[c]	7.83	8.47	5.78	5.94	5.13	5.42	5.21	5.02	5.48	4.89	5.49	5.60
17	A″ (π → π*)	2.43	8.19[c]	9.50	9.97	9.98	9.18	7.31	7.87	7.83	7.53	7.60	8.15	7.75	7.55
18	A (π → π*)	0.36	0.42[c]	1.24	0.85	11.66[a]	1.61	0.60	0.81	0.64	0.62	0.48	0.55	0.56	0.60
19	A (π → π*)	2.38	6.48[c]	8.72	8.56	11.92	8.27	5.52	6.17	5.53	5.00	5.58	4.90	5.38	5.47
20	A (π → π*)	2.25	6.17[c]	8.55	8.89	13.18	9.74	6.10	6.54	6.23	5.57	3.74	5.77	6.03	6.00
21	A (π → π*)	1.09	2.81[c]	2.89	3.84	1.73	2.29	2.89	2.72	2.38	2.28	2.73	1.70	2.71	3.05
22	A (π → π*)	**4.13**	**17.13**[c]	**21.62**	**21.78**	**17.33**	**19.82**	**15.27**	**17.21**	**15.95**	**14.06**	**16.46**	**14.20**	**14.87**	**14.80**
23	A (n → π*)	0.43	*1.42*[c]	*1.73*	*1.84*	*2.36*	*1.88*	*1.00*	*1.49*	*1.58*	*1.56*	*1.61*	*1.71*	*1.37*	*1.23*
	B (π → π*)	0.47	1.21[c]	1.40	1.40	0.50	0.97	1.59	1.05	1.03	1.01	1.05	0.72	0.94	1.00
24[b]	A (π → π*)	1.42	3.69[c]	*3.64*	*5.59*	3.27	3.46	3.42	3.39	3.24	3.24	3.52	2.84	3.07	3.11
25[b]	B_2 (π → π*)	0.05	0.09[c]	0.23	0.20	0.65	0.31	0.05	0.12	0.09	0.03	0.02	0.26	0.06	0.02

[a] State mixing between two closely lying π → π* states. [b] Dipole moments were determined at the center of mass for the charged molecules, this does not affect Δμ. [c] Dipole moments were estimated using the following formula: $\mu_{CCSD}^{cc\text{-}pVTZ^*} = \mu_{CCSD}^{cc\text{-}pVDZ} + \left(\mu_{CC2}^{cc\text{-}pVTZ} - \mu_{CC2}^{cc\text{-}pVDZ}\right)$. [d] BSE/ev*GW*/PBE0 (FF). [e] BSE/ev*GW*/PBE0 (AA). [f] BSE/ev*GW*/PBEh (AA). [g] BSE/ev*GW*/PBEα (AA).

Table 3 Statistical analysis of the excess dipole moments presented in Table 2. The CCSD (OR) data was used as a reference for the statistical analysis. All values but R, ρ, and R^2 are in Debye

	CC2 (OR)	ADC(2) (OR)	PBE[a]	PBE0	PBEh	M06-2X	CAM-B3LYP	ωB97X-D	BSE/*GW* PBE0[b]	BSE/*GW* PBE0[c]	BSE/*GW* PBEh[d]	BSE/*GW* PBEα[e]
MAE	1.03	1.21	2.42	1.44	0.79	0.68	0.79	0.90	0.75	1.16	0.77	0.71
MSE	0.93	1.19	0.95	0.35	−0.40	−0.18	−0.33	−0.50	−0.28	−0.75	−0.42	−0.33
σ	1.15	1.16	3.38	1.99	0.95	0.93	0.95	1.03	0.96	1.48	0.92	0.85
Max(+)	4.49	4.65	8.26	3.79	1.27	1.74	1.35	1.14	1.20	1.45	1.08	0.95
Max(−)	−0.77	−0.11	−7.05	−5.46	−2.18	−2.67	−2.52	−3.07	−2.57	−5.71	−2.26	−2.33
R	0.98	0.99	0.69	0.89	0.98	0.98	0.98	0.98	0.97	0.95	0.98	0.98
ρ	0.93	0.95	0.63	0.81	0.90	0.92	0.90	0.92	0.91	0.89	0.92	0.92
R^2	0.96	0.97	0.47	0.79	0.95	0.95	0.95	0.96	0.95	0.90	0.96	0.96

[a] The problematic case of molecule **18** was removed from the data set for the statistical analysis with the PBE functional. [b] BSE/ev*GW*/PBE0 (FF). [c] BSE/ev*GW*/PBE0 (AA). [d] BSE/ev*GW*/PBEh (AA). [e] BSE/ev*GW*/PBEα (AA).

BSE/ev*GW* $\Delta\mu$ are either on the same level of accuracy as the TD-DFT using a RSH XCF or a bit closer from the CCSD values.

In order to have a more general view of the accuracy of different methods, a statistical analysis of the $\Delta\mu$ is given in Table 3 (see statistics for μ^{ES} in the ESI†). We used CCSD (OR) values as a benchmark for the statistics since it is the highest affordable level of theory. However, we have also performed a statistical analysis using CC2 data as a reference in the ESI.† In Table 3 we can see that the smallest MAE, MSE, and σ values are obtained with TD-M06-2X, BSE/evGW/PBE0 (FF), and BSE/evGW/PBEα (AA) approaches, whereas both CC2 and ADC(2) OR approaches yield larger deviation. Additionally, statistical analysis of the μ^{GS} and μ^{ES} (see Tables S18 and S19 in the ESI†) shows larger MAE and σ for both CC2 and ADC(2) than TD-DFT (PBEh, M06-2X, CAM-B3LYP, and ωB97X-D) and BSE/ev*GW*. This indicates that the small errors obtained with the latter methods for the $\Delta\mu$ are not coming from the error compensation of the two dipoles. TD-PBE provides the highest MAE (2.42 D) and a large σ (Table 3): the TD-PBE dipoles are quite inconsistent. As expected, CC2 and ADC(2) give MAE, MSE, and σ that are very close to each other: when OR is used the two methods provide similar properties. TD-PBEh, TD-M06-2X, TD-CAM-B3LYP, TD-ωB97X-D, and BSE/ev*GW* provide negative MSE, hinting at an underestimation trend for these methods, which can also be seen from the Max(+) and Max(−), where TD-DFT (except PBE and PBE0) and BSE/ev*GW* methods show small (less than 1.8 D) maximal positive deviations, but quite significant maximal negative deviations. In contrast, quite large Max(+) and Max(−) errors are observed for TD-PBE and TD-PBE0 levels of theory. In Table 3 both Pearson (R) and Spearman (ρ) coefficients are also given, both evaluating the correlation between two sets of data; the direction of the correlation being either a positive (maximum of +1) or negative (maximum of −1). The difference between the two is that the first measures the linear correlation whereas the second assesses how two variables can be related by a monotonic function. Our results show that we have very strong positive linear and monotonic correlations for all methods (except for TD-PBE) presented in Table 3: chemical trends are accurately reproduced. The lowest values for both ρ and R are obtained for the TD-PBE and TD-PBE0 methods, while for all other methods, both coefficients are close to 1. However, it is seen that both TD-PBE and TD-PBE0 show a higher correlation with the reference values for the μ^{ES}. We also provide the linear determination coefficient (R^2) and the best R^2 among DFT functionals is obtained with TD-PBEh, TD-M06-2X, and RSH functionals that provide determination coefficients very close to each other (0.95–0.96). BSE/ev*GW*/PBE0 (FF) and BSE/ev*GW*/PBEα (AA) also deliver alike R^2. In the case of μ^{ES}, the statistics of Table S19 (ESI†) indicates that all BSE/ev*GW* analytical dipoles show higher determination coefficients compared to the ones calculated using the finite-field approach. Additionally, TD-PBEh and BSE/ev*GW*/PBEh (AA) statistical results are quite similar for $\Delta\mu$, while the clear advantage of the latter is observed for μ^{ES} (Table S19, ESI†). To sum up, TD-PBE and TD-PBE0 show inconsistent errors in predicting $\Delta\mu$ due to the mix of overestimation and underestimation trends, while more consistent results can be obtained with TD-M06-2X, TD-CAM-B3LYP, and TD-ωB97X-D. BSE/ev*GW*/PBE0 $\Delta\mu$ obtained with approximate analytical gradient tends to be less accurate than the ones determined by finite differences, but using an improved starting point such as tuned PBEα functionals leads to AA results closer from the FF ones. A comparison of the data between BSE/ev*GW* (AA) PBE0 and PBEα data shows that the starting point dependency is more pronounced for $\Delta\mu$ (average of 34% difference), μ^{ES} (average of 13% difference), and f (average of 11% difference) than for ΔE (average of 3% difference). In short, BSE/ev*GW* provides both $\Delta\mu$ and μ^{ES} equivalent or slightly more accurate than TD-DFT using an appropriate functional.

4 Conclusions

In the present contribution we studied the accuracy of the BSE/*GW* formalisms for the calculation of dipole moments, more specifically we focused on the difference between the ES and GS dipole moments, *i.e.*, excess dipoles ($\Delta\mu$) as well as ES dipoles (μ^{ES}). We benchmarked the $\Delta\mu$ and μ^{ES} obtained with CC2, ADC(2), TD-DFT, and BSE/*GW* levels of theory using CCSD as reference. In the first part, the accuracy of the excess and ES dipole evolutions for the two lowest singlet ES of DMABN

during the twist of the amino group was studied. Our results show that, for the **1B** ES, significant differences are observed between CC2 and CCSD levels of theory. This is connected to the fact that CC2 underestimates the transition energies and does not show the same behavior for the two lowest B ES as CCSD. In this case, TD-DFT functionals, except TD-PBEh, are following the CC2 trends, while BSE/ev*GW* mimics the CCSD behavior. Additionally, we showed that the BSE/ev*GW* formalism provides consistent trends for the differences between **1B** and **2A** total $\Delta\mu$ values (that are close to the CCSD results), whereas with TD-DFT this is only achieved with TD-PBEh. It turns out that the ev*GW* scheme is less effective in removing the starting point dependency for both $\Delta\mu$ and μ^{ES} than for energies. In the second part of this work, the accuracy of TD-DFT and BSE/ev*GW* $\Delta\mu$ values was assessed for a set of 25 dyes of various ES characters. Our results show that the accuracy of BSE/*GW* is globally on the same level or slightly better than that of TD-DFT relying on M06-2X and RSH functionals. Moreover, in a few challenging cases (zwitterionic and cyanine transitions) BSE/*GW* outperforms TD-DFT. Additionally, we tested the accuracy of the recently proposed efficient but approximated analytical gradient scheme to compute BSE/*GW* dipole moments: it usually provides slightly underestimated values as compared to the non-approximated approach and requires the use of an adequate starting point such as the optimally-tuned PBEα functional in order to achieve a good agreement with the reference finite-field values.

Conflicts of interest

There are no conflicts to declare.

Acknowledgements

The authors are indebted to the French Agence Nationale de la Recherche (ANR) under contract ANR-20-CE29-0005 (BSE-Forces) for financial support. I. K. is thankful to the EUR LUMOMAT program and the Investments for the Future program (contract ANR-18-EURE-0012) for their support. The authors are thankful for the generous allocations of time by the CCIPL computational center installed in Nantes and by the national HPC facilities (contract GENCI-TGCC A0110910016).

References

1 W. Liptay, *Angew. Chem., Int. Ed. Engl.*, 1969, **8**, 177–188.
2 M. Iida, Y. Ohshima and Y. Endo, *J. Phys. Chem.*, 1993, **97**, 357–362.
3 C. Han, Z. Zhang, D. Ding and H. Xu, *Chem*, 2018, **4**, 2154–2167.
4 E. Lippert, W. Ludar and H. Boss, *Advances in Molecular Spectroscopy*, Pergamon Press, Oxford, 1962.
5 K. Rotkiewicz, K. Grellmann and Z. Grabowski, *Chem. Phys. Lett.*, 1973, **19**, 315–318.
6 Z. R. Grabowski, K. Rotkiewicz and W. Rettig, *Chem. Rev.*, 2003, **103**, 3899–4032.
7 C. Wang, W. Chi, Q. Qiao, D. Tan, Z. Xu and X. Liu, *Chem. Soc. Rev.*, 2021, **50**, 12656–12678.
8 I. Georgieva, A. J. A. Aquino, F. Plasser, N. Trendafilova, A. Köhn and H. Lischka, *J. Phys. Chem. A*, 2015, **119**, 6232–6243.
9 J. R. Lombardi, *Spectrochim. Acta, Part A*, 1987, **43**, 1323–1324.
10 M. Schmitt and L. Meerts, *Frontiers and Advances in Molecular Spectroscopy*, Elsevier, 2018, pp. 143–193.
11 E. Lippert, *Z. Naturforsch., A: Phys. Sci.*, 1955, **10**, 541–545.
12 N. Mataga, Y. Kaifu and M. Koizumi, *Bull. Chem. Soc. Jpn.*, 1956, **29**, 465–470.
13 E. G. McRae, *J. Phys. Chem.*, 1957, **61**, 562–572.
14 F. W. Fowler, A. R. Katritzky and R. J. D. Rutherford, *J. Chem. Soc. B*, 1971, 460–469.
15 T. Abe, *Bull. Chem. Soc. Jpn.*, 1991, **64**, 3224–3228.
16 A. Chrayteh, A. Blondel, P.-F. Loos and D. Jacquemin, *J. Chem. Theory Comput.*, 2021, **17**, 416–438.
17 G. D. Purvis and R. J. Bartlett, *J. Chem. Phys.*, 1982, **76**, 1910–1918.
18 H. Koch, H. J. A. Jensen, P. Jørgensen, T. Helgaker, G. E. Scuseria, I. Schaefer and F. Henry, *J. Chem. Phys.*, 1990, **92**, 4924–4940.
19 O. Christiansen, H. Koch and P. Jørgensen, *Chem. Phys. Lett.*, 1995, **243**, 409–418.
20 J. Schirmer, *Phys. Rev. A: At., Mol., Opt. Phys.*, 1982, **26**, 2395–2416.
21 A. Dreuw and M. Wormit, *Wiley Interdiscip. Rev.: Comput. Mol. Sci.*, 2015, **5**, 82–95.
22 T. Helgaker, P. Jørgensen and N. C. Handy, *Theor. Chim. Acta*, 1989, **76**, 227–245.
23 O. Christiansen, P. Jørgensen and C. Hättig, *Int. J. Quantum Chem.*, 1998, **68**, 1–52.
24 M. Kállay and J. Gauss, *J. Chem. Phys.*, 2004, **121**, 9257–9269.
25 D. J. Rowe, *Rev. Mod. Phys.*, 1968, **40**, 153–166.
26 J. F. Stanton and R. J. Bartlett, *J. Chem. Phys.*, 1993, **98**, 7029–7039.
27 J. Schirmer, *Phys. Rev. A: At., Mol., Opt. Phys.*, 1991, **43**, 4647–4659.
28 J. Schirmer and F. Mertins, *Theor. Chem. Acc.*, 2010, **125**, 145–172.
29 E. A. Salter, H. Sekino and R. J. Bartlett, *J. Chem. Phys.*, 1987, **87**, 502–509.
30 G. W. Trucks, E. Salter, C. Sosa and R. J. Bartlett, *Chem. Phys. Lett.*, 1988, **147**, 359–366.
31 M. Hodecker, D. R. Rehn, A. Dreuw and S. Höfener, *J. Chem. Phys.*, 2019, **150**, 164125.
32 R. Sarkar, M. Boggio-Pasqua, P.-F. Loos and D. Jacquemin, *J. Chem. Theory Comput.*, 2021, **17**, 1117–1132.
33 E. Runge and E. K. U. Gross, *Phys. Rev. Lett.*, 1984, **52**, 997–1000.
34 M. E. Casida, in *Time-Dependent Density Functional Response Theory for Molecules*, ed. D. P. Chong, World Scientific, Singapore, 1995, vol. 1, pp. 155–192.

35 C. Adamo and D. Jacquemin, *Chem. Soc. Rev.*, 2013, **42**, 845–856.
36 R. A. King, *J. Phys. Chem. A*, 2008, **112**, 5727–5733.
37 M. R. Silva-Junior, M. Schreiber, S. P. A. Sauer and W. Thiel, *J. Chem. Phys.*, 2008, **129**, 104103.
38 C. A. Guido, D. Jacquemin, C. Adamo and B. Mennucci, *J. Phys. Chem. A*, 2010, **114**, 13402–13410.
39 M. R. Silva-Junior and W. Thiel, *J. Chem. Theory Comput.*, 2010, **6**, 1546–1564.
40 D. Jacquemin, *J. Chem. Theory Comput.*, 2016, **12**, 3993–4003.
41 E. E. Salpeter and H. A. Bethe, *Phys. Rev.*, 1951, **84**, 1232–1242.
42 G. Csanak, H. Taylor and R. Yaris, *Advances in Atomic and Molecular Physics*, Academic Press, 1971, vol. 7, pp. 287–361.
43 W. Hanke and L. J. Sham, *Phys. Rev. Lett.*, 1979, **43**, 387–390.
44 G. Strinati, *Riv. Nuovo Cimento*, 1988, **11**, 1–86.
45 M. Rohlfing and S. G. Louie, *Phys. Rev. Lett.*, 1998, **81**, 2312–2315.
46 S. Albrecht, L. Reining, R. Del Sole and G. Onida, *Phys. Rev. Lett.*, 1998, **80**, 4510–4513.
47 L. X. Benedict, E. L. Shirley and R. B. Bohn, *Phys. Rev. Lett.*, 1998, **80**, 4514–4517.
48 X. Blase, I. Duchemin, D. Jacquemin and P.-F. Loos, *J. Phys. Chem. Lett.*, 2020, **11**, 7371–7382.
49 L. Hedin, *Phys. Rev.*, 1965, **139**, A796–A823.
50 M. S. Hybertsen and S. G. Louie, *Phys. Rev. B: Condens. Matter Mater. Phys.*, 1986, **34**, 5390–5413.
51 R. W. Godby, M. Schlüter and L. J. Sham, *Phys. Rev. B: Condens. Matter Mater. Phys.*, 1988, **37**, 10159–10175.
52 D. Golze, M. Dvorak and P. Rinke, *Front. Chem.*, 2019, **7**, 377.
53 I. Duchemin, T. Deutsch and X. Blase, *Phys. Rev. Lett.*, 2012, **109**, 167801.
54 B. Baumeier, D. Andrienko and M. Rohlfing, *J. Chem. Theory Comput.*, 2012, **8**, 2790–2795.
55 P. Cudazzo, M. Gatti, A. Rubio and F. Sottile, *Phys. Rev. B: Condens. Matter Mater. Phys.*, 2013, **88**, 195152.
56 P. Boulanger, D. Jacquemin, I. Duchemin and X. Blase, *J. Chem. Theory Comput.*, 2014, **10**, 1212–1218.
57 V. Ziaei and T. Bredow, *J. Chem. Phys.*, 2016, **145**, 174305.
58 D. Jacquemin, I. Duchemin and X. Blase, *J. Phys. Chem. Lett.*, 2017, **8**, 1524–1529.
59 X. Blase, I. Duchemin and D. Jacquemin, *Chem. Soc. Rev.*, 2018, **47**, 1022–1043.
60 X. Gui, C. Holzer and W. Klopper, *J. Chem. Theory Comput.*, 2018, **14**, 2127–2136.
61 F. Kaplan, M. E. Harding, C. Seiler, F. Weigend, F. Evers and M. J. van Setten, *J. Chem. Theory Comput.*, 2016, **12**, 2528–2541.
62 T. Rangel, S. M. Hamed, F. Bruneval and J. B. Neaton, *J. Chem. Theory Comput.*, 2016, **12**, 2834–2842.
63 S. Ismail-Beigi and S. G. Louie, *Phys. Rev. Lett.*, 2003, **90**, 076401.
64 M. S. Kaczmarski and M. Rohlfing, *J. Phys. B: At., Mol. Opt. Phys.*, 2010, **43**, 051001.
65 M. S. Kaczmarski, Y. Ma and M. Rohlfing, *Phys. Rev. B: Condens. Matter Mater. Phys.*, 2010, **81**, 115433.
66 D. Jacquemin, I. Duchemin, A. Blondel and X. Blase, *J. Chem. Theory Comput.*, 2016, **12**, 3969–3981.
67 O. Çaylak and B. Baumeier, *J. Chem. Theory Comput.*, 2021, **17**, 879–888.
68 I. Knysh, I. Duchemin, X. Blase and D. Jacquemin, *J. Chem. Phys.*, 2022, **157**, 194102.
69 I. Knysh, K. Letellier, I. Duchemin, X. Blase and D. Jacquemin, *Phys. Chem. Chem. Phys.*, 2023, **25**, 8376–8385.
70 I. Knysh, J. D. J. Villalobos-Castro, I. Duchemin, X. Blase and D. Jacquemin, *J. Phys. Chem. Lett.*, 2023, **14**, 3727–3734.
71 T. Helgaker and P. Jørgensen, *Theor. Chim. Acta*, 1989, **75**, 111–127.
72 F. Furche and R. Ahlrichs, *J. Chem. Phys.*, 2002, **117**, 7433–7447.
73 J. Villalobos-Castro, I. Knysh, D. Jacquemin, I. Duchemin and X. Blase, *J. Chem. Phys.*, 2023, **159**, 024116.
74 C. Hättig and F. Weigend, *J. Chem. Phys.*, 2000, **113**, 5154–5161.
75 E. Epifanovsky, A. T. B. Gilbert, X. Feng, J. Lee, Y. Mao, N. Mardirossian, P. Pokhilko, A. F. White, M. P. Coons, A. L. Dempwolff, Z. Gan, D. Hait, P. R. Horn, L. D. Jacobson, I. Kaliman, J. Kussmann, A. W. Lange, K. U. Lao, D. S. Levine, J. Liu, S. C. McKenzie, A. F. Morrison, K. D. Nanda, F. Plasser, D. R. Rehn, M. L. Vidal, Z.-Q. You, Y. Zhu, B. Alam, B. J. Albrecht, A. Aldossary, E. Alguire, J. H. Andersen, V. Athavale, D. Barton, K. Begam, A. Behn, N. Bellonzi, Y. A. Bernard, E. J. Berquist, H. G. A. Burton, A. Carreras, K. Carter-Fenk, R. Chakraborty, A. D. Chien, K. D. Closser, V. Cofer-Shabica, S. Dasgupta, M. de Wergifosse, J. Deng, M. Diedenhofen, H. Do, S. Ehlert, P.-T. Fang, S. Fatehi, Q. Feng, T. Friedhoff, J. Gayvert, Q. Ge, G. Gidofalvi, M. Goldey, J. Gomes, C. E. González-Espinoza, S. Gulania, A. O. Gunina, M. W. D. Hanson-Heine, P. H. P. Harbach, A. Hauser, M. F. Herbst, M. Hernández Vera, M. Hodecker, Z. C. Holden, S. Houck, X. Huang, K. Hui, B. C. Huynh, M. Ivanov, A. Jasz, H. Ji, H. Jiang, B. Kaduk, S. Kähler, K. Khistyaev, J. Kim, G. Kis, P. Klunzinger, Z. Koczor-Benda, J. H. Koh, D. Kosenkov, L. Koulias, T. Kowalczyk, C. M. Krauter, K. Kue, A. Kunitsa, T. Kus, I. Ladjanszki, A. Landau, K. V. Lawler, D. Lefrancois, S. Lehtola, R. R. Li, Y.-P. Li, J. Liang, M. Liebenthal, H.-H. Lin, Y.-S. Lin, F. Liu, K.-Y. Liu, M. Loipersberger, A. Luenser, A. Manjanath, P. Manohar, E. Mansoor, S. F. Manzer, S.-P. Mao, A. V. Marenich, T. Markovich, S. Mason, S. A. Maurer, P. F. McLaughlin, M. F. S. J. Menger, J.-M. Mewes, S. A. Mewes, P. Morgante, J. W. Mullinax, K. J. Oosterbaan, G. Paran, A. C. Paul, S. K. Paul, F. Pavošević, Z. Pei, S. Prager, E. I. Proynov, A. Rak, E. Ramos-Cordoba, B. Rana, A. E. Rask, A. Rettig, R. M. Richard, F. Rob, E. Rossomme, T. Scheele, M. Scheurer, M. Schneider, N. Sergueev, S. M. Sharada, W. Skomorowski, D. W. Small, C. J. Stein, Y.-C. Su, E. J. Sundstrom, Z. Tao, J. Thirman, G. J. Tornai, T. Tsuchimochi, N. M. Tubman, S. P. Veccham, O. Vydrov, J. Wenzel, J. Witte, A. Yamada, K. Yao, S. Yeganeh, S. R. Yost, A. Zech, I. Y. Zhang, X. Zhang, Y. Zhang, D. Zuev, A. Aspuru-

Guzik, A. T. Bell, N. A. Besley, K. B. Bravaya, B. R. Brooks, D. Casanova, J.-D. Chai, S. Coriani, C. J. Cramer, G. Cserey, I. DePrince, A. Eugene, J. DiStasio, A. Robert, A. Dreuw, B. D. Dunietz, T. R. Furlani, I. Goddard, A. William, S. Hammes-Schiffer, T. Head-Gordon, W. J. Hehre, C.-P. Hsu, T.-C. Jagau, Y. Jung, A. Klamt, J. Kong, D. S. Lambrecht, W. Liang, N. J. Mayhall, C. W. McCurdy, J. B. Neaton, C. Ochsenfeld, J. A. Parkhill, R. Peverati, V. A. Rassolov, Y. Shao, L. V. Slipchenko, T. Stauch, R. P. Steele, J. E. Subotnik, A. J. W. Thom, A. Tkatchenko, D. G. Truhlar, T. Van Voorhis, T. A. Wesolowski, K. B. Whaley, I. Woodcock, H. Lee, P. M. Zimmerman, S. Faraji, P. M. W. Gill, M. Head-Gordon, J. M. Herbert and A. I. Krylov, *J. Chem. Phys.*, 2021, **155**, 084801.

76 TURBOMOLE V7.5.1 2021, a development of University of Karlsruhe and Forschungszentrum Karlsruhe GmbH, 1989-2007, TURBOMOLE GmbH, since 2007; available from **https://www.turbomole.org**.

77 S. G. Balasubramani, G. P. Chen, S. Coriani, M. Diedenhofen, M. S. Frank, Y. J. Franzke, F. Furche, R. Grotjahn, M. E. Harding, C. Hättig, A. Hellweg, B. Helmich-Paris, C. Holzer, U. Huniar, M. Kaupp, A. Marefat Khah, S. Karbalaei Khani, T. Müller, F. Mack, B. D. Nguyen, S. M. Parker, E. Perlt, D. Rappoport, K. Reiter, S. Roy, M. Rückert, G. Schmitz, M. Sierka, E. Tapavicza, D. P. Tew, C. van Wüllen, V. K. Voora, F. Weigend, A. Wodyński and J. M. Yu, *J. Chem. Phys.*, 2020, **152**, 184107.

78 M. J. Frisch, G. W. Trucks, H. B. Schlegel, G. E. Scuseria, M. A. Robb, J. R. Cheeseman, G. Scalmani, V. Barone, G. A. Petersson, H. Nakatsuji, X. Li, M. Caricato, A. V. Marenich, J. Bloino, B. G. Janesko, R. Gomperts, B. Mennucci, H. P. Hratchian, J. V. Ortiz, A. F. Izmaylov, J. L. Sonnenberg, D. Williams-Young, F. Ding, F. Lipparini, F. Egidi, J. Goings, B. Peng, A. Petrone, T. Henderson, D. Ranasinghe, V. G. Zakrzewski, J. Gao, N. Rega, G. Zheng, W. Liang, M. Hada, M. Ehara, K. Toyota, R. Fukuda, J. Hasegawa, M. Ishida, T. Nakajima, Y. Honda, O. Kitao, H. Nakai, T. Vreven, K. Throssell, J. A. Montgomery, Jr., J. E. Peralta, F. Ogliaro, M. J. Bearpark, J. J. Heyd, E. N. Brothers, K. N. Kudin, V. N. Staroverov, T. A. Keith, R. Kobayashi, J. Normand, K. Raghavachari, A. P. Rendell, J. C. Burant, S. S. Iyengar, J. Tomasi, M. Cossi, J. M. Millam, M. Klene, C. Adamo, R. Cammi, J. W. Ochterski, R. L. Martin, K. Morokuma, O. Farkas, J. B. Foresman and D. J. Fox, *Gaussian-16 Revision A.03*, Gaussian Inc., Wallingford CT, 2019.

79 J. P. Perdew, K. Burke and M. Ernzerhof, *Phys. Rev. Lett.*, 1997, **78**, 1396.

80 C. Adamo and V. Barone, *J. Chem. Phys.*, 1999, **110**, 6158–6170.

81 T. Yanai, D. P. Tew and N. C. Handy, *Chem. Phys. Lett.*, 2004, **393**, 51–57.

82 I. Duchemin and X. Blase, *J. Chem. Theory Comput.*, 2020, **16**, 1742–1756.

83 I. Duchemin and X. Blase, *J. Chem. Theory Comput.*, 2021, **17**, 2383–2393.

84 X. Ren, P. Rinke, V. Blum, J. Wieferink, A. Tkatchenko, A. Sanfilippo, K. Reuter and M. Scheffler, *New J. Phys.*, 2012, **14**, 053020.

85 F. Weigend, A. Köhn and C. Hättig, *J. Chem. Phys.*, 2002, **116**, 3175–3183.

86 F. Neese, F. Wennmohs, U. Becker and C. Riplinger, *J. Chem. Phys.*, 2020, **152**, 224108.

87 T. Le Bahers, C. Adamo and I. Ciofini, *J. Chem. Theory Comput.*, 2011, **7**, 2498–2506.

88 D. Jacquemin, T. L. Bahers, C. Adamo and I. Ciofini, *Phys. Chem. Chem. Phys.*, 2012, **14**, 5383–5388.

89 D. Jacquemin, I. Duchemin and X. Blase, *J. Chem. Theory Comput.*, 2015, **11**, 5340–5359.

90 Y. Zhao and D. G. Truhlar, *Theor. Chem. Acc.*, 2008, **120**, 215–240.

91 J.-D. Chai and M. Head-Gordon, *Phys. Chem. Chem. Phys.*, 2008, **10**, 6615–6620.

92 P. Wiggins, J. A. G. Williams and D. J. Tozer, *J. Chem. Phys.*, 2009, **131**, 091101.

93 D. A. Matthews and J. F. Stanton, *J. Chem. Phys.*, 2016, **145**, 124102.

